Chapter 3

Sonolytic Conversion of the Aqueous Perfluorinated Surfactants, Perfluorooctanoate (PFOA) and Perfluorooctanesulfonate (PFOS) into Inorganic Constituents

Sections reprinted with permission from Vecitis, C. D.; Park H.; Cheng J.; Mader, B. T.; Hoffmann, M. R. *Journal of Physical Chemistry A* **2008**, *112*, 4261–4270.

Abstract

The perfluorinated surfactants perfluorooctane sulfonate (PFOS) and perfluorooctanoate (PFOA) are recognized as widespread in the environment as well as recalcitrant towards most conventional water treatment technologies. In this study acoustic cavitation as driven by high-frequency ultrasound is shown to be effective in the degradation of aqueous solutions of PFOS and PFOA, and effective over a wide range of concentrations from 10 nM to 10 μM for a given compound. Sulfur, fluorine, and carbon mass balances indicate that mineralization occurs immediately following the degradation of the initial perfluorinated surfactant. Near-complete conversion of PFOS and PFOA to CO, CO_2, F^-, and SO_4^{2-} occurs due to pyrolytic reactions at the surface and vapor phase of transiently collapsing cavitation bubbles. The initial PFOS or PFOA pyrolytic degradation occurs at the bubble-water interface and involves the loss of the ionic functional group leading to the formation of the corresponding 1H-fluoroalkane or perfluoroolefin. The fluorochemical intermediates undergo a series of pyrolytic reactions in the bubble vapor leading to C_1 fluoro-radicals. Secondary vapor-phase bimolecular reactions coupled with concomitant hydrolysis converts the C_1 fluoro-radicals to carbon monoxide, carbon dioxide and HF, forming a proton and fluoride upon dissolution. Sonochemical half-lives, which are calculated from high-temperature gas-phase kinetics, are consistent with kinetic observations and suggest that mineralization occurs shortly after an initial perfluorinated surfactant interfacial pyrolysis.

Introduction

Over the last 60 years, fluorochemicals (FCs) have been used for a wide variety of applications such as water-proofing of materials, protective coating of metals, fire-fighting foams for electrical and grease fires, semi-conductor etching, and lubrication. The widespread use of these compounds is due to their favorable physical properties, which include chemical stability, low coefficients of friction, and low polarizabilities (i.e., fluorophilicity)[1]. The same properties that make FCs valuable as commercial products make them difficult to treat using most conventional environmental remediation strategies or waste treatment technologies[2–4]. For example, Schultz et al.[3] reported that the total mass of PFOA and PFOS is not reduced (i.e., is resistant to physical and biological treatments) during conventional wastewater treatment processes. Consequently, fluorochemicals have become widespread in the environment[5–7].

Most conventional degradation technologies are ineffective for the *in situ* degradation of aqueous PFOS and PFOA, present in the aqueous phase, since they are inherently recalcitrant to chemical and microbiological treatment[2,3,8–11]. Advanced oxidation processes (AOPs)[12], which utilize the hydroxyl radical, such as UV-ozonation[13], peroxone (i.e., a mixture of O_3 and H_2O_2)[13], or Fenton's reagent (i.e., H_2O_2 and Fe^{2+} salts)[13–15] have been shown to be ineffective for PFOA and PFOS destruction. A number of photolytic methods such as direct photolysis[15–20], persulfate photolysis[16,21–23], alkaline isopropanol photolysis[19] and photocatalysis[15,24–28] have shown varying degrees of efficacy on higher concentrations of perfluorocarboxylates. However, none of these methods lead to the mineralization of PFOS and PFOA. Reduction by elemental iron under near-super-critical water conditions has been shown to be possible for PFOS degradation[29]. However, scale-up of high-pressure, high-temperature treatment systems is

difficult[30]. Moriwaki et al.[14] have shown that ultrasonic irradiation of aqueous solutions can degrade these compounds with fluoride and sulfate as the primary degradation products.

Sonochemistry, as induced by ultrasonic irradiation of aqueous solutions at near-ambient temperatures and pressures, has been shown to be effective for the treatment of a wide variety of chemical contaminants[31–35]. Ultrasonic pressure waves force the formation and quasi-adiabatic collapse of vapor bubbles formed from pre-existing gas nuclei[36]. The transient collapse of aqueous cavitation bubbles has been shown through chemical methods to raise average internal vapor temperatures near 4000 K[37–39] and are supported by single-bubble collapse models[40–42], while bubble-water interface temperatures have been calculated to be in the range of 600 to 1000 K[34]. These transient high temperatures lead to *in situ* pyrolytic reactions in the vapor and interfacial regions of each collapsing bubble, resulting in the breakdown of water-producing hydroxyl radicals ($^{\cdot}OH$), oxygen atoms (O), and hydrogen atoms ($H^{\cdot}$). These transient radicals react readily with compounds in the bubble gas-phase or at the bubble interface. Some of the radical species are dispersed into the bulk solution by nonspherical bubble collapse. Ultrasonic degradation is effective for the removal of contaminants with high Henry's Law constants[43–45] that partition into the vapor phase of the bubble, or for chemical contaminants which partition to the air-water interface[46–48] such as PFOS and PFOA[14].

We hereby report a detailed investigation into the kinetics and mechanism of the sonochemical conversion of aqueous PFOS and PFOA to inorganic constituents.

Experimental Methods

Ammonium perfluorooctanoate (APFO) and potassium perfluorooctanesulfonate (PFOS) standards, consisting of a mixture of branched and linear isomers, were provided

by 3M Company. Ammonium acetate (> 99 %) and methanol (HR-GC > 99.99 %) were obtained from EMD Chemicals, Inc. Aqueous solutions were prepared with purified water using a Milli-Q system (18.2 MΩ cm^{-1} resistivity).

Sonications at frequencies of 354 and 618 kHz were performed using an Allied Signal Elac Nautik ultrasonic transducer (23.6 cm^2) at an applied power of 150 W with the solution contained in a 600 mL jacketed glass reactor. The temperature was controlled with a Neslab RTE-111 refrigerated bath maintained at 10 ºC. Sonications performed at 500 kHz were completed with an Undatim ultrasonic transducer (25.5 cm^2) at an applied power of 75 W with the solution contained in a 400 mL jacketed glass reactor. The temperature was controlled with a Haake A80 refrigerated bath set to 10 ^oC. All reactions were sparged with argon for at least 30 minutes prior to reaction. Initial solution pH was between 7 and 8 for all reactions. Calorimetry was done to determine the acoustic power transferred to solution. At 354, 500, and 618 kHz the applied (calorimetric) power densities in W L^{-1} were 250 (200), 150 (128), and 250 (208), respectively. The applied acoustic power densities will be referred to in the text.

A number of reactor configurations, initial concentrations, and mixtures were used for the various experiments. PFOS and PFOA were analyzed for in all experiments by an HPLC-MSD-Ion Trap (Agilent). Fluoride and sulfate were analyzed by ion chromatography (Dionex) and completed using 618 kHz, 250 W L^{-1}, and 6.4 W cm^{-2} on a closed system where the produced gas was resparged into solution to retain all products: PFOS and PFOA were sonicated separately at initial concentrations of approximately 10 μM. Trace gas analyses by GC-MS (Agilent) and FT-IR (Midac) were sonicated at 500 kHz, 150 W L^{-1}, and 2.9 W cm^2 on a closed system where the headspace was recirculated but not resparged through a 300 mL multiple reflection FT-IR cell with an in-line valved

port for GC-MS sampling: PFOS and PFOA were sonicated simultaneously at a total initial concentration of 20 μM (10 μM each). The experiments where CO and CO_2 were measured during sonication were completed using 354 kHz, 250 W L^{-1} and 6.4 W cm^{-2} using a continuously sparged (100 to 125 mL min^{-1}) open system where the product gas was evacuated (≈ 100 mL min^{-1}) into a high-vacuum chamber through a stainless-steel membrane inlet to be analyzed by EI-MS (Balzers): PFOS and PFOA were sonicated separately at initial concentrations of 100 μM. Reactor configurations and analytical procedures are detailed in the supporting information.

Results

Ultrasonic irradiation degradation kinetics of aqueous PFOS, $[PFOS]_i$ = 200 nM , and PFOA, $[PFOA]_i$ = 240 nM are plotted in Figure 3.1 (υ = 358 kHz, ρ_{PD} = 250 W L^{-1}, I_P = 6.4 W cm^{-2}). The observed kinetics are quasi-exponential (i.e., the ln ($[PFOX]_t/[PFOX]_i$) vs. time plot is linear) and is typical of what would be expected for PFOS and PFOA co-contamination in an environmental system where concentrations are in the picomolar to micromolar range[7]. Apparent pseudo-first-order kinetics are given in eq. 3.1

$$\frac{d[PFOX]}{dt} = -k_{app}^{-PFOX}[PFOX] \tag{3.1}$$

where X = A or S and [PFOX] are the representative carboxylate or sulfonate concentrations and k_{app}^{-PFOX} are the apparent first-order rate constants for each species. A linear fit of the kinetic plots gives k_{app}^{-PFOA} = 0.041 min^{-1} ($\tau_{1/2}$ = 16.9 minutes) and k_{app}^{-PFOS} = 0.027 min^{-1} ($\tau_{1/2}$ = 25.7 minutes). The PFOA degradation rate constant is 1.5 times that of PFOS. The observed pseudo-first-order kinetics are in agreement with results previously reported by Moriwaki et al.[14] for the sonolytic degradation (200 kHz and 3 W cm^{-2}) of aqueous PFOS and PFOA at 20 and 24 μM, respectively. Similar sonochemical

kinetics were also observed for hydrocarbon surfactants such as Triton X-100[32] and linear alkyl benzyl sulfonates[49].

A time-dependent sulfur mass balance for an aqueous PFOS solution where $[PFOS]_i$ = 10 μM was obtained at ultrasonic conditions of 618 kHz, 250 W L^{-1}, and 6.4 W cm^{-2}. The PFOS sulfur mass balance is shown in Figure 3.2 in units of moles sulfur per each species over total initial moles of PFOS sulfur. Aqueous sulfate ion, as detected by ion chromatography, was the only observed sulfur-containing product and has a formation half-life equivalent to the PFOS degradation half-life and thus is formed as PFOS is initially destroyed. At each point in time, the total sulfur balance, given by the sum of sulfate and PFOS sulfur, is equal to or greater than one.

The corresponding mass balance for fluorine of aqueous PFOS, $[PFOS]_i$ = 10 μM, and PFOA, $[PFOA]_i$ = 12 μM, during sonication for the same conditions is shown in Figure 3.3 in terms of moles fluorine per species over total initial moles PFOX fluorine. In earlier work, Moriwaki et al. detected low-levels of shorter-chain perfluoro-acids as reaction intermediates during the sonolytic degradation of PFOS and PFOA[14]; however, we did not detect any of these intermediates during our experiments. Aqueous fluoride accounted for greater than 90% of the fluorine from the degraded PFOS and PFOA at any point in time during the reaction, as shown in Figures 3.3a and b, respectively.

The solid line through the PFOS, PFOA, sulfate, and fluoride data points shown in Figures 3.2 and 3.3 are obtained from kinetic analyses. For example, the PFOA fluorine mass balance data is fit using eq. 3.2

$$\frac{\{moles\ F\}_{PFOA,t}}{\{moles\ F\}_{PFOA,i}} = \exp(-k_1^{-PFOA}t) \qquad (3.2)$$

while the fluoride and sulfate mass balance data are fit to a double exponential involving a single intermediate decay, (e.g., PFOS $\rightarrow$ I $\rightarrow$ F^- or SO_4^{2-}). k_1^{-PFOX}, as determined from eq. 3.2, is the rate constant for the initial decay, PFOS $\rightarrow$ I, and $k_2^{X^-}$ is the rate constant for the second decay, I $\rightarrow$ F^- or SO_4^{2-}. For example, $k_2^{SO_4^{2-}}$ is determined through fitting the sulfate-normalized mass balance data to eq. 3.3.

$$\frac{\{moles\ S\}_{SO_4^{2-},t}}{\{moles\ S\}_{PFOS,i}} = \frac{1}{k_1^{-PFOS} + k_2^{SO_4^{2-}}}(k_2^{SO_4^{2-}}(1-\exp(-k_1^{-PFOS}t)) - k_1^{-PFOS}(1-\exp(-k_2^{SO_4^{2-}}t))) \quad (3)$$

The rate constants determined from the kinetic fits are given in Table 3.1. The PFOS and PFOA sonochemical decomposition rate constants decrease slightly at the somewhat higher initial concentrations used in the mass balance experiments as compared to those shown in Figure 3.1. The intermediate, I, conversion rate constant to sulfate, $k_2^{SO_4^{2-}}$, is > 1 min^{-1}, thus the sulfonate moiety ($-CF_2-SO_3^-$) is converted quantitatively to sulfate (SO_4^{2-}) shortly after the PFOS decomposition, $-d[PFOS]/dt \approx d[SO_4^{2-}]/dt$. This suggests that the sonolytic decomposition of PFOS proceeds via pyrolytic C-S bond cleavage[50] to yield an oxysulfur intermediate such as SO_3 or SO_3F^- which is readily hydrolyzed or oxidized to SO_4^{2-}. A similar mechanism is expected for PFOA sonolysis where the initial bond cleavage occurs at the carbon-carbon bond between the carboxylate group and the fluorinated tail, $R_FCF_2-CO_2^-$, releasing CO_2[51,52]. Initial ionic headgroup cleavage mechanism should produce a fluorinated alkane or alkene as the other primary sonolysis intermediate. These are transformed to F^- at a rate constant of 0.3 min^{-1} for both PFOS and PFOA, suggesting a similar fluoride production pathway for both species. The slower rate of fluoride production as compared to sulfate production during PFOS sonolysis is consistent with an initial C-S bond cleavage mechanism producing a fluorinated alkane

intermediate that requires multiple, sequential pyrolytic steps prior to fluoride production[53].

The time-dependent sulfur and fluorine measurements are also consistent with the analysis of headspace gases by multiple reflection FT-IR and GC-MS during simultaneous sonication of PFOS and PFOA, $[PFOS]_i$ = 10 μM and $[PFOA]_i$ = 10 μM (500 kHz, 188 W L^{-1} and 2.9 W cm^{-2}). A large number of fluorinated gases were detected by GC-MS of the reactor headspace which was captured in an evacuated cannister. The gases that were detected include 1) polyfluorinated alkanes, CHF_3, CH_2F_2, CH_3F, C_2F_5H, C_3F_7H, 2) polyfluorinated alkenes, $C_2F_2H_2$, C_2F_4, C_3F_6, C_4F_8, and 3) C_4-C_8 polyfluorinated alkenes. No sulfur-containing gases were detected. The most abundant of the fluorinated gas species were fluoroform and difluoromethane, whose gas concentrations were monitored by online multiple reflection FT-IR (Figure 3.4: note the scale of the y-axis is a factor of 10^4 lower than that of Figure 3.3 at all points in time). The maximum concentration of these two species amounted to < 0.1% of the total fluorine during the simultaneous sonolysis of PFOS and PFOA. After these gas-phase products were formed, they were reentrained into the aqueous phase destroyed by continued sonolysis. However, these species were not completely eliminated since the headspace was not resparged back into the reactor, as the experiment was designed to accumulate any intermediate fluorochemicals for detection. Thus, passive gas transfer back into the sonicated solution was the limiting kinetic step of fluoroform and difluoromethane degradation. A table of all of the trace species detected by GC-MS after 120 minutes of sonolysis is listed in the supporting information: the total fluorine mole fraction of these species is 0.005 or less than 1%.

A carbon mass balance for the sonolytic degradation of PFOA and PFOS is plotted in Figures 3.5a and b as moles of carbon per species over the total initial moles of carbon vs. time, $[PFOS]_i$ = 100 μM and $[PFOA]_i$ = 100 μM (354 kHz, 250 W L^{-1}, and 6.4 W cm^{-2}). The primary carbon-containing species were the initial surfactant as detected by HPLC-MS and CO and CO_2, which were detected using real-time EI-MS. Other possible gaseous intermediates including formaldehyde, carbonyl fluoride, HF did not exceed the limit of detection. Real-time mass spectrometry was used to reduce the effect of any secondary gas product oxidation, $CO_{(g)} \rightarrow CO_{2(g)}$, or reduction/thermolysis, $CO_{2(g)} \rightarrow CO_{(g)}$[54,55], that may occur in subsequent bubble collapse events. After 120 minutes of sonolysis, 64.6 ± 9.2% of the carbon from decomposed PFOA was converted to CO and 32.1 ± 7.0% was converted to CO_2, while, in the case of PFOS sonolysis, the conversions to CO and CO_2 are 74.0 ± 5.3 % and 14.6 ± 5.0%, respectively, yielding observed product ratios of $[CO]/[CO_2]_{PFOA}$ = 2.0 and $[CO]/[CO_2]_{PFOS}$ = 5.1.

Discussion

Interfacial Pyrolysis of the Initial Perfluorinated Surfactant

PFOS and PFOA are surfactants[56–59]. PFOS is considered to be a more effective surfactant since it has one more carbon than PFOA in its perfluorinated tail. Their surfactant properties coupled with their small Henry's constants (Table 3.2) precludes their diffusive transfer to the bubble vapor phase. These properties are consistent with sonochemical degradation at the bubble-water interface[14] Oxidation by hydroxyl radicals[32,47] at collapsing bubble-water interfaces is a possible mechanism. An upper limit for the second-order rate constant for the reaction of hydroxyl radical, $< 10^6$ $M^{-1}s^{-1}$, with both PFOA and PFOS has been estimated by analogy to the measured rate constant of hydroxyl radical reacting with trifluoroacetate. For comparison, oxalate ($C_2O_4^{2-}$),

which is thought to be responsible for the slow TOC elimination during sonication[60], has a second-order rate constant with hydroxyl radical of 4.7 x 10^7 $M^{-1}s^{-1}$; which is at least an order of magnitude greater than that of PFOS and PFOA. TOC elimination, and thus oxalate oxidation, has a sonolytic half-life under similar conditions of ten hours[60]. Given these arguments, hydroxyl radical oxidation appears to play a minor role in PFOS and PFOA degradation[14]. Thus, interfacial pyrolytic decomposition appears to be the primary pathway for the sonochemical degradation of the perfluorinated surfactants.

Interfacial pyrolysis can be broken down conceptually into two fundamental steps. The first step involves the diffusion and adsorption of PFOS or PFOA to a transiently cavitating bubble interface (Step 1, Scheme 3.1) followed by a second step involving pyrolytic degradation at the cavitating-bubble interface (Step 2, Scheme 3.1).

The time-dependent mass balances shown in Figures 3.2–3.5 provide some insight into the sonolytic degradation mechanism of PFOS and PFOA. Of particular interest is the almost immediate production of inorganic sulfur (sulfate) and fluorine (fluoride) contrasted with a slightly delayed production of CO and CO_2. This suggests that

$$\frac{-d[PFOX]}{dt} = \frac{d(Mineralization)}{dt} \tag{3.4}$$

and that the primary intermediates produced during PFOS and PFOA decomposition appear to have much shorter half-lives than precursors. Given these observations, it is clear that

$$\frac{d[PF-Intermediate]}{dt} >> \frac{d[PFOX]}{dt} \tag{3.5}$$

and that the decomposition of the perfluoro-intermediates occurs in the vapor phase. Sonochemical reactions involving species that can partition to the vapor phase of a collapsing bubble (i.e., those having high Henry's constants) generally have the fastest

degradation rates. The similarity between the fluorochemical surfactant degradation rates and the rates of mineralization suggests that the fluorointermediates formed from the initial pyrolytic reactions have high Henry's constants.

Pyrolysis of perfluorinated surfactants has been reported for several perfluoroalkanecarboxylates and perfluoroalkanesulfonates in the solid phase[50,52,61] and perfluoroalkanecarboxylates in the vapor phase[51,62]. The primary products of perfluoroalkanecarboxylate pyrolysis product are reported to be the analogous 1H-perfluoroalkanes (eq. 3.6) for NH_4^+ salts[52,62], and perfluoroolefins (eq. 3.7) with lesser amounts of perfluoroanhydrides and perfluoroacyl fluorides for alkaline and alkali salts[52].

$$CF_3(CF_2)_6COO^-NH^+_{4(s)} \xrightarrow{\Delta} CF_3(CF_2)_5CF_2H_{(g)} + CO_{2(g)} + NH_{3(g)} \quad (3.6)$$

$$CF_3(CF_2)_6COO^-K^+_{(s)} \xrightarrow{\Delta} CF_3(CF_2)_4CF = CF_{2(g)} + CO_{2(g)} + K^+F^-{}_{(s)} \quad (3.7)$$

Products generated during the thermal degradation of perfluorosulfonates have not been identified[50]. Ammonium perfluorooctanoate, which is thermally converted to the 1H-perfluoroalkane[52,62], decomposes at a temperature 50 to 100 K lower than that of the alkali and alkaline salts[50,52,61]. Excess water has been observed to have an effect on the Arrhenius parameters of PFOA-NH_4^+ thermolysis[62] by increasing log A values from 13.6 s^{-1} to 15.4 s^{-1} and activation energy from 150 kJ mol^{-1} to 172 kJ mol^{-1}. These activation energies are much lower than expected for the $–CF_2$-CF_2- bond breaking which are typically > 300 kJ mol^{-1} (Table 3.3). Initial cleavage of the C-C bond between the perfluorinated tail and the carboxylate group yields gaseous carbon dioxide and a perfluoroalkyl anion (eq. 3.8). The perfluoroanion can form a 1H-perfluoroalkane by proton transfer (eq. 3.9), which eliminates a C-F bond-breaking step (450 kJ mol^{-1}) and circumvents the perfluoroolefin formation pathway (eq. 3.10).

$$CF_3(CF_2)_6COO^- \xrightarrow{\Delta} CF_3(CF_2)_5CF_2^- + CO_{2(g)} \quad (3.8)$$

$$CF_3(CF_2)_5CF_2^- \xrightarrow{+H_2O} CF_3(CF_2)_5CF_2H + HO^- \quad (3.9)$$

$$CF_3(CF_2)_5CF_2^- \xrightarrow{\Delta} CF_3(CF_2)_4CF = CF_2 \quad (3.10)$$

A proton transfer mechanism can explain the lower decomposition temperatures of the ammonium salts (eq. 3.6) as compared to the alkali and alkaline salts (eq. 3.7). Typical thermal decomposition of similar perfluoroalkane-carboxylate and -sulfonate salts[50] indicates that sulfonate salts decompose at higher temperatures (e.g., 100 to 200 K higher) than corresponding carboxylate salts. These observations are consistent with the relative sonolytic degradation rates of PFOA (k_{app}^{-PFOA} = 0.041 min^{-1}) and PFOS (k_{app}^{-PFOS} = 0.027 min^{-1}), in spite of the greater interfacial activity and tendencies of PFOS.

In summary, initial PFOX decomposition involves the loss of the ionic headgroup: CO_2 in the case of PFOA, and SO_3 in the case of PFOS. The pyrolytic cleavage of the ionic headgroups of both molecules leads to the formation of C_7 and C_8 perfluorocarbanion intermediates for PFOA and PFOS, respectively. The perfluorocarbanion is protonated to form a 1H-perfluoroalkane (eq. 3.9) or undergoes fluoride elimination to form a perfluoroolefin (eq. 3.10), (Step 2, Scheme 3.1). SO_3 produced during PFOS decomposition hydrolyzes rapidly (Step 3, Scheme 3.1) to form sulfate with the release of two protons.

Unimolecular Decomposition of the Fluorocarbon Tail

The organo-fluorines in the C_7 and C_8 fluorochemical intermediates are sonochemically converted into F^- with a pseudo-first-order rate constant of 0.3 min^{-1} ($\tau_{1/2}$

= 2.3 min). The fluorochemical intermediate degradation rates are greater than the sonochemical degradation rates reported for chlorinated hydrocarbons[63,64]. The Henry's constants for the likely 1H-perfluoroalkane (eq. 3.9) and perfluoroolefin (eq. 3.10) intermediates have been estimated by two different methods and determined to be on the order of 10^5 to 10^6 atm L mol^{-1} (Table 3.1). Colussi et al.[45] established a correlation between the Henry's constant, K_{A-W}^{x}, for chlorinated hydrocarbons, x, and their apparent sonolytic degradation rate constants where: $k_{sono,app}^{-x} = 4.5 \times 10^{-3} \; K_{A-W}^{x\;0.3}$ (s^{-1}). Given the range of Henry's constants for the perfluorointermediates, we estimate sonolytic half-lives from 1 to 3 s; these times are shorter but consistent with the observed fluoride production kinetics ($\tau_{1/2}$ = 140 s). Partitioning of fluororocarbons between phases can not be estimated accurately using parameters determined for hydrocarbons[65–67]. For example, measurement[66] of Henry's constants for perfluoroolefins is difficult. The perfluoro-intermediates may not immediately partition into the vapor phase rapidly, but dwell for a period of time at the bubble-water interface before pyrolytic vapor-phase decomposition.

The apparent discrepancy between the observed F^- production rates and estimated degradation rates of these fluoro-intermediates may be due to a greater number of acoustic cycles to produce F^-, CO, and CO_2. The unimolecular decomposition kinetics for C_7 and C_8 fluorocarbon-intermediates in question have not been determined experimentally or computationally. Instead, we will use kinetic parameters for shorter-chain fluorochemicals in order to estimate decomposition rates.

Pyrolytic kinetics of (experimental technique listed in parentheses) 1H-perfluoropropane (IRMPD)[68], 1-perfluorobutene (IRMPD)[69], perfluorohexane (VLPP)[53],

and their decomposition intermediates are listed in Table 3.3. First-order rate constants and half-lives are estimated using a temperature of 2500 K, which is less than the average vapor temperature achieved during a single transient cavitation event[37,39,70,71] in water. At 2500 K, experimentally determined Arrhenius parameters should be valid. It is noted that all of the possible fluorocarbon-intermediates have at least one estimated C-C bond-breaking decomposition pathway with a half-life under 100 ps, and the subsequent fluoroalkyl radical intermediates all have faster C-C bond-breaking kinetics. The unimolecular decomposition kinetics will dominate the bimolecular reaction kinetics and we can assume that the initial fluoro-intermediate will dissociate into C_1 fluoro-radical constituents prior to any intervening bimolecular reactions.

In Scheme 3.2, we propose a degradation mechanism for perfluorooctene in a cavitating bubble. The values above the reaction arrows are the estimated times for greater than 99% of the reaction. The stoichiometries for 1H-perfluoroheptane and perfluorooctene decompositions are given in eqs. 3.11 and 3.12, respectively.

$$CF_3(CF_2)_5CF_2H \xrightarrow{\Delta} CF_3 + 5\ CF_2 + CF_2H \tag{3.11}$$

$$CF_3(CF_2)_5CF = CF_2 \xrightarrow{\Delta} CF_3 + 6\ CF_2 + CF \tag{3.12}$$

The C_1 fluoro-radical products retain their original C-F bond intact since the average –C-C- bond strength (410 kJ mol^{-1}) is substantially less than the average C-F bond strength (530 kJ mol^{-1}). For comparison, the O-H bond strength of water is 498 kJ mol^{-1}.

Numerical simulations by Yasui et al.[42] and Colussi et al.[40] have modeled the time-dependent temperature evolution and the subsequent chemical reactions taking place during a transiently cavitation event at 300 kHz. In both cases, the maximum bubble-vapor temperatures were above 2500 K. Under these conditions, the characteristic time for the reactions portrayed in Scheme 3.2 to take place is 1 ns. Therefore, the C_7 or C_8

fluoro-intermediates should be completely dissociated into C_1 fluoro-radical constituents in a single acoustic cycle.

Transformation of C_1 Fluoro-radical Intermediates into CO and CO_2

The initial sonochemical decomposition steps of PFOS and PFOA produce either C_7 or C_8 1H-perfluoroalkanes (eq. 3.9) or perfluoroolefins (eq. 3.10), (Step 2, Scheme 3.1). These intermediates are then pyrolytically decomposed into C_1 fluoro-radicals (eqs. 3.11, 3.12): trifluoromethyl radical ($\cdot CF_3$), difluoromethyl radical ($\cdot CHF_2$), fluoromethylidyne (CF), and difluorocarbene ($:CF_2$), (Step 4, Scheme 3.1). The C_1 fluoro-radicals are subsequently transformed into carbon monoxide and carbon dioxide. A series of bimolecular reactions with H_2O, $H\cdot$, $HO\cdot$, and O-atom are proposed in Table 3.4 for the conversion of the C_1 fluoro-radicals into CO, CO_2, and HF[72]. The second-order reaction rate constants are estimated at 4000 K, where H_2O thermolysis is significant. Several assumptions are made when estimating the high-temperature kinetics. First, it is assumed that the radical intermediates constitute a neglible fraction of the total bubble vapor content; as a consequence fluoro-radical/fluoro-radical reactions can be neglected. Second, the C_1 fluoro-radical unimolecular decomposition is assumed to be of minor importance, since at aqueous cavitation temperatures[39,70], the thermolytic splitting of water, which has a lesser bond strength than fluoro-radical C-F bonds, is dominant. Finally, the sonolytic interconversion of CO and CO_2[48,54] is assumed to be insignificant since $CO_2 \xrightarrow{)))} CO$ has a half-life on the order of one hour under similar conditions[54]. Furthermore, if interconversion of CO and CO_2 were significant during sonolysis, then the CO/CO_2 product ratios for PFOS and PFOA would be similar; however, we observe $[CO]/[CO_2]_{PFOA} = 2.0$ and $[CO]/[CO_2]_{PFOS} = 5.1$.

The branching ratios for the pyrolytic transformations of the C_1 fluoro-radicals can be calculated using relative H_2O, H·, HO·, and O-atom vapor concentrations estimated from numerical simulations of single bubble cavitation events[40–42]. Storey and Szeri[41] (26.5 kHz, 1.2 bar, Ar) calculate that the bubble will be 14 % water vapor upon reaching its minimum radius and they predict that H_2O, H·, HO·, and O-atom are the dominate chemical species. Yasui et al.[42] (300 kHz, 3.0 bar, air) calculate that the bubble will have 10 to 20% water vapor before and after the bubble reaches a minimum size, while H·, HO·, and O-atom concentrations range from 0.1 to 1.0 % of the bubble contents during temperature maximums. Colussi et al.[40] (300 kHz, 1.8 atm, Ar) have calculated that HO·, H·, and O-atom concentrations are dissimilar during bubble radius minima at 1.0, 0.1, and 0.01 % of the total bubble gas content, respectively.

The [CO]/[CO_2] product ratios for PFOS and PFOA sonolysis are estimated in three cases using relative C_1 fluoro-radical and their secondary C_1 intermediate branching ratios at various concentrations of H_2O, H·, HO·, and O-atom, as shown in Table 3.5. In the first case, H·, HO·, and O-atom concentrations are all set to 1%, in the second case H·, HO·, and O-atom are set to 0.1% and in the final case HO·, H·, and O-atom are set to 1.0%, 0.1%, and 0.01%, respectively. For all three cases, vapor concentrations were set at 10%, 1.0%, or 0.1%. The primary transformation pathways (i.e., those with branching ratios > 0.01) are shown in Scheme 3.3 with the primary reactant listed above the reaction arrow.

In Table 3.5 are the bubble vapor conditions used for the estimations, the CO/CO_2 branching ratios, for the secondary C_1 intermediates, the PFOS and PFOA estimated CO/CO_2 branching ratios and the estimated branching ratio over the experimentally determined branching ratio. The bubble vapor conditions that result in a best fit to the

experimental data were 10% water vapor and 1% or 0.1% H·, HO·, and O-atom. When a range of radical concentrations were varied, the CO/CO_2 branching ratios were underestimated by 55 to 80%. This underestimation was primarily due to the reduced H· vapor concentration, H·/HO· = 0.1, yielding a more oxidizing bubble vapor and thus the more oxidized carbon product, CO_2. The CO/CO_2 branching ratios for CFO and CF_2O are observed to favor CO_2 over CO upon decreasing H· concentration. Reducing the relative water vapor concentration increases the CO branching ratio of CF_2O.

An analagous calculation as presented above for the unimolecular decomposition of the initial fluorochemical intermediate can be used to estimate the number of acoustic cycles, or sonication time, for the C_1 fluoroadicals in Scheme 3.3 to completely pyrolyze into CO and CO_2. If we considered the reaction with the longest half-life, $COF_2 + H_2O \rightarrow CO_2 + 2\ HF$, at 8.15 μs (4000 K, 10% H_2O), and that eight half-lives are needed to destroy > 99% of the initial compound, the time for complete transformation would be 65 μs. Using a conservative 0.50 ns high temperature period per cycle, it will take 1.3×10^5 acoustic cycles to completely eliminate COF_2. Likewise, the total time for the sonolytic transformation of the C_1-fluororadical is estimated to be 0.36 s (2.8 μs per cycle at 354 kHz). The calculated time is inline with the characteristic degradation time (e.g., 1 to 3 s) using the empirical Henry's constant estimation[45]. And once again this calculation is in general agreement, but much shorter, than the experimentally observed fluoride production half-life of 2 minutes. The discrepancy between calculation and experiment suggests that fluorochemical intermediates partitioning to the bubble vapor phase and not pyrolytic degradation may be the rate-limiting step in fluoride production. More importantly, both experimental results and kinetic estimations agree with the conclusion that shortly after the sonochemical decomposition of a perfluorinated surfactant, PFOS or

PFOA, their fluoro-intermediates are transformed relatively quickly into inorganic constituents of PFOX: F^-, SO_4^{2-}, CO, and CO_2.

Conclusions

Perfluorinated surfactants are widespread in the environment and recalcitrant towards most conventional water-treatment technologies. Incineration is a viable method for degradation of concentrated manufacturing wastes, yet not efficient for more dilute aqueous solutions. Acoustic cavitation as driven by ultrasonic cavitation has been shown to be both an effective and a relatively fast method for the complete destruction and mineralization of PFOS and PFOA over a wide range of initial concentrations. Conventional methods such as hydroxyl radical oxidation[13] and bio-degradation[8] have been shown to have minimal effect on the elimination on these compounds from water. Photodegradation techniques[15,16,21,22,24,26] as well as elemental iron reduction in sub-critical water[29] have been shown to degrade these species. However, minimum degradation half-lives are in the range of 45 to 120 minutes and achieve a maximum of 50% mineralization. Shorter perfluorinated acids are produced as by-products; these latter products are just as recalcitrant as the initial perfluorinated compounds. The PFOS and PFOA degradation rates presented here both have a degradation half-life of 30 minutes or less and achieve complete mineralization immediately after the decomposition of the initial product, as shown by time-dependent product analysis and kinetic estimations. Previous studies[73] have shown that sonolytic rates can be scaled linearly by increasing acoustic power density and that scaling-up the reactor size has minimal effect on the observed reaction rates. Therefore, ultrasonically driven acoustic cavitation provides a technically viable method for the treatment of aqueous perfluorinated

surfactant waste waters over a rather wide range of concentrations (i.e., 10 nM (5 ppb) to 10 mM (5 ppm) in this study).

Figures

Figure 3.1. Pseudo-first-order plots of PFOX sonolysis (354 kHz, 250 W L^{-1}, Ar, 10 ^{o}C, $[PFOS]_i$ = 200 nM, $[PFOA]_i$ = 240 nM). PFOS (○) and PFOA (∇)

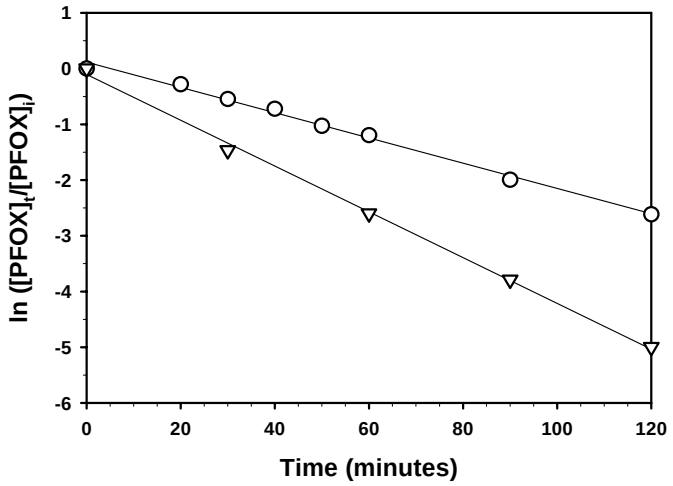

Figure 3.2. Normalized sulfur mass balance during PFOS sonolysis. (618 kHz, 250 W L^{-1},Ar,10 ^{o}C, $[PFOS]_i$ = 10 μM). PFOS (●), sulfate (○) and sulfate + PFOS (▼)

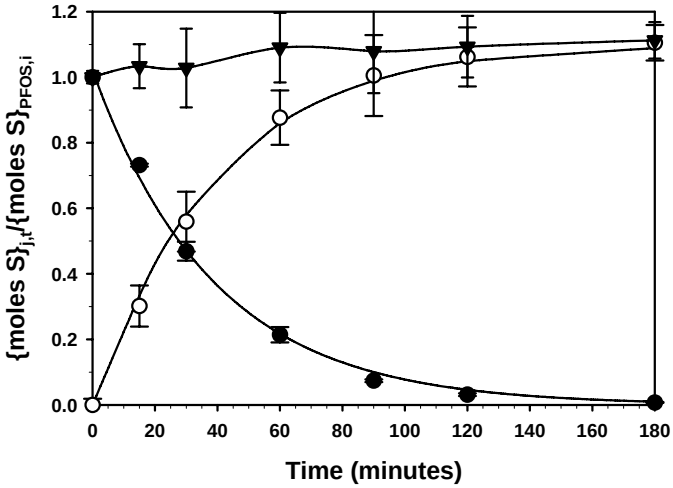

Figure 3.3. Normalized fluorine mass balance during PFOX sonolysis (618 kHz, 250 W L^{-1}, Ar, 10 ^{o}C). **A)** $[PFOS]_i$ = 10 μM; PFOS (●), fluoride (○), and PFOS + fluoride (▼). **B)** $[PFOA]_i$ = 12 μM; PFOA (●), fluoride (○) and PFOA + fluoride (▼).

A

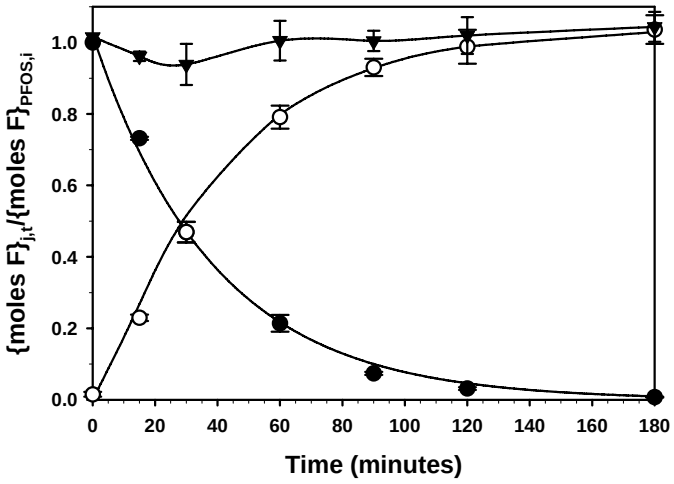

B

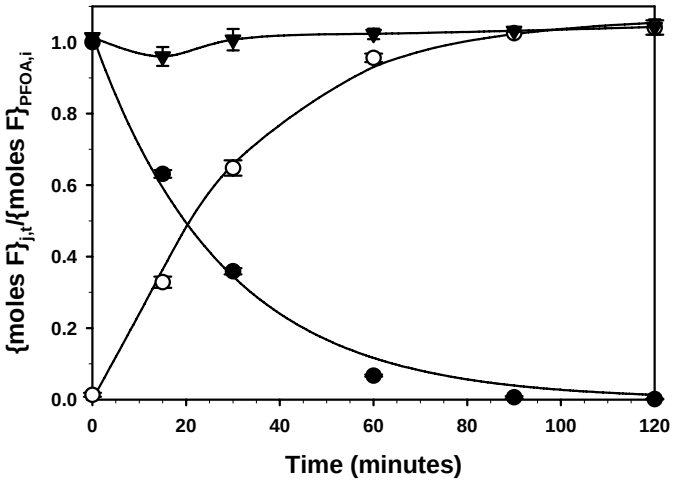

Figure 3.4. Trace gases, CH_2F_2 and CHF_3, detected during PFOX sonolysis (500 kHz, 188 W L^{-1}, Ar, 10 ^oC, $[PFOS]_i$ = 10 μM and $[PFOA]_i$ = 12 μM). CH_2F_2 (○) and CHF_3 (●)

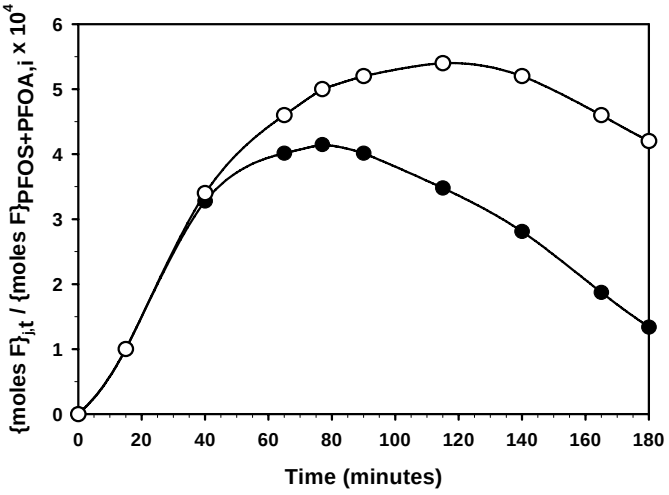

Figure 3.5. Normalized carbon mass balance plots during PFOX sonolysis (354 kHz, 250 W L^{-1}, Ar, 10 ^{o}C). A) $[PFOS]_i$ = 100 μM; PFOS (◊), CO (○), CO_2 (∇), CO + CO_2 (□), and PFOS + CO + CO_2 (♦). B) $[PFOA]_i$ = 100 μM; PFOA (◊), CO (○), CO_2 (∇), CO + CO_2 (□), and PFOA + CO + CO_2 (♦)

A

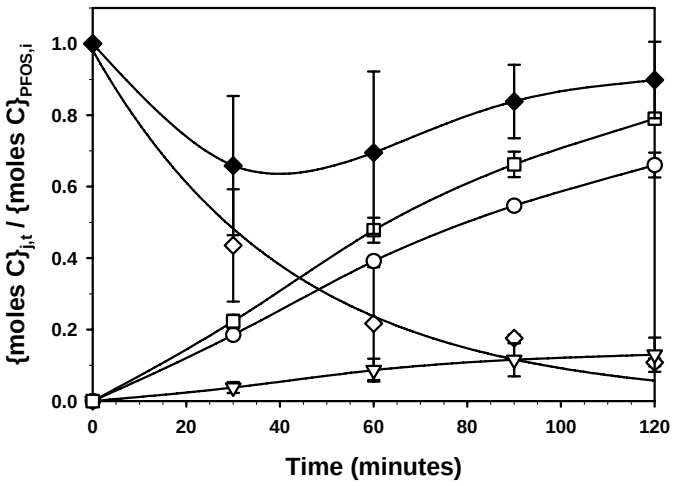

B

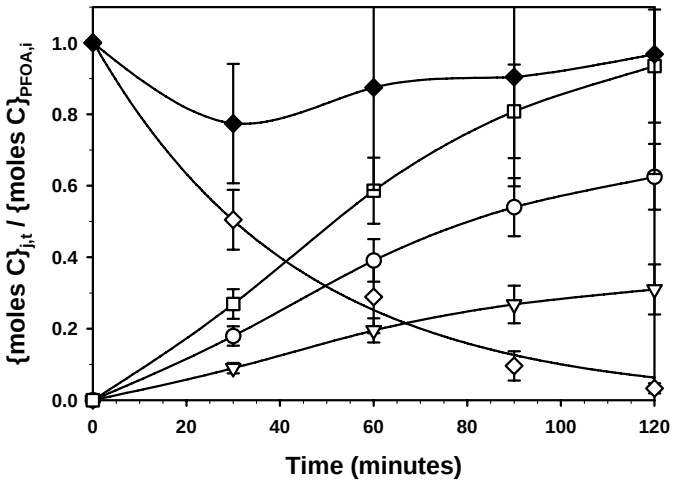

Schemes

Scheme 3.1. A representative scheme of the sonochemical PFOS transformation into its inorganic constituents. Step 1) PFOS adsorption to the bubble-water interface; Step 2) Bubble-water interfacial pyrolytic decomposition of PFOS via cleavage of the C-S bond; Step 3) Hydrolysis of sulfur trioxide to sulfate; Step 4) Bubble vapor pyrolysis of the primary fluoro-intermediate into C_1 fluoro-radicals; and Step 5) Transformation of C_1 fluoro-radicals within the bubble vapor to CO, CO_2, and HF, which is converted to a proton and a fluoride upon hydration. The inorganic products are highlighted in purple boxes.

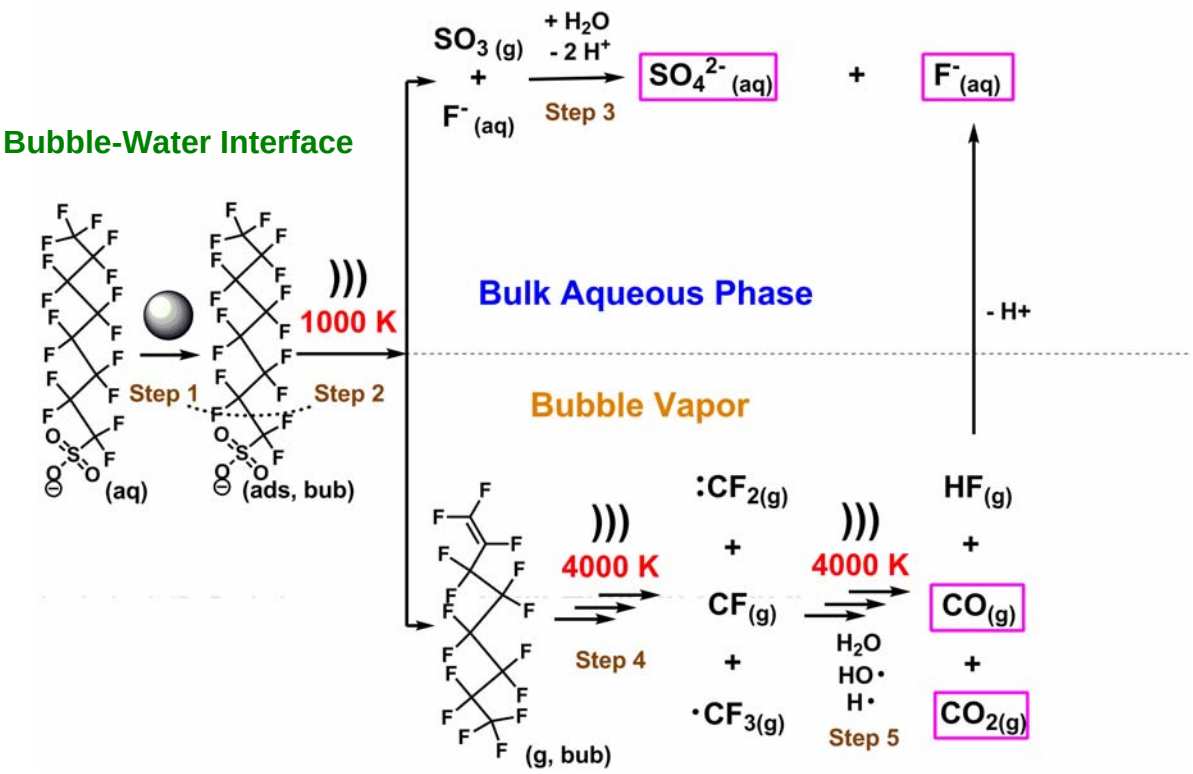

Scheme 3.2. A representative scheme of sonolytic fluorointermediate unimolecular decomposition yielding C_1 fluoro-radicals (Step 4, Scheme 3.1). The time for > 99 % reaction progress at 2500 K is reported above the reaction arrow. The C_1 fluoro-radicals are shown in boxes.

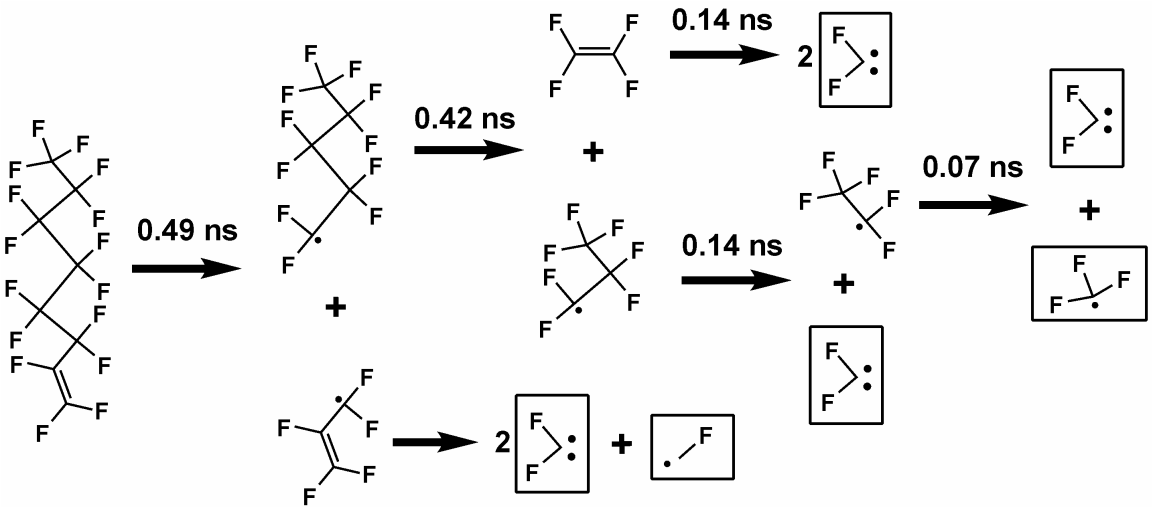

Scheme 3.3. Representation of sonochemical C_1-fluorointermediate reaction pathways (Step 5, Scheme 3.1). The initial C_1 fluoro-radicals are in boxes and the final products are in ovals. The bimolecular reactant is listed either above the reaction arrow or to the right of vertical reaction arrows. If multiple reactants are listed they signify multiple individual pathways and not sequential reactions.

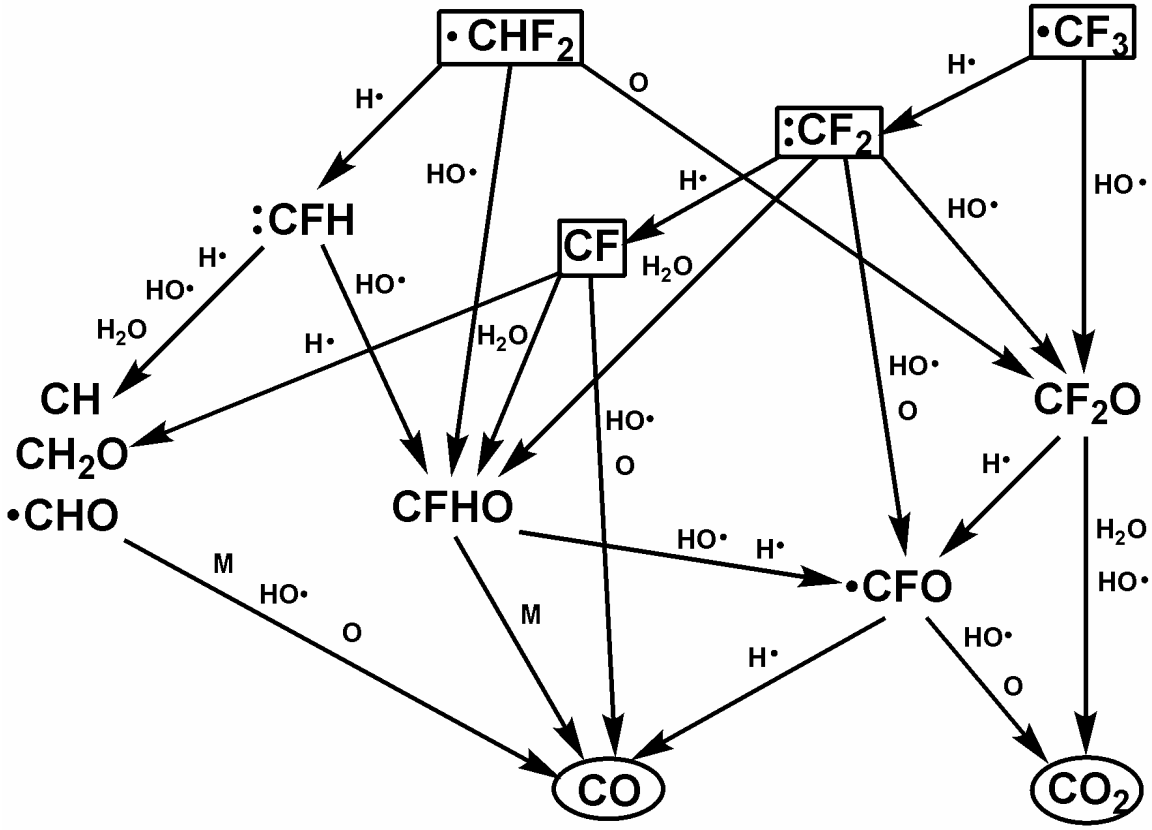

Tables

Table 3.1. Rate constants for PFOX sonochemical transformations

	k_1^{-PFOX} (min^{-1})[a]	$k_2^{F^-}$ (min^{-1})[b]	$k_2^{SO_4^{2-}}$ (min^{-1})[b]
PFOS	0.026	0.3	> 1.0
PFOA	0.036	0.3	

a) PFOX fluorine and sulfur sonochemical time dependence was fit to an exponential decay: exp(-k_1^{-PFOX} t).

b) Inorganic fluorine, fluoride, and sulfur, sulfate, sonochemical time-dependent growth was fit to exponential growth through a single decomposition intermediate: (1/($k_1^{-PFOX} + k_2^{X^-}$))($k_2^{X^-}$ (1-exp(-k_1^{-PFOX} t))- k_1^{-PFOX} (1-exp(-$k_2^{X^-}$ t))).

Table 3.2. Physiochemical properties of PFOX sonochemical intermediates

	$C_{w,sat}$ (M) 20 °C	p* (atm) 20 °C	K_H (atm M^{-1})	pKa	$k_{\cdot OH}$
PFOS-K^{+1}	0.002	3.3 x 10^{-9}	N/A	-3.5	< 10^{6} [a]
PFOA-NH_4^+	0.05 (gels)	9.2 x 10^{-8}	N/A	-0.5[67]	< 10^{6} [a]
PF-Octene	1.4 x 10^{-8} [74]	0.03	2.1 x 10^{6}	n/a	2.4 x 10^{-12} [b]
1H-PF-Octane	n/a	n/a	6.2 x 10^{6} [d]	n/a	10$^{-9.2}$e$^{-63/RT}$ [c]
PF-Heptene	1.4 x 10^{-7}	0.075	5.3 x 10^{5}	n/a	2.4 x 10^{-12} [b]
1H-PF-Heptane	3.5 x 10^{-8} [75]	0.04	3.3 x 10^{5}	n/a	10$^{-9.2}$e$^{-63/RT}$ [c]

*Vapor pressures for the fluorochemical intermediates are estimated according to Mackay et al.[76]

*$C_{w,sat}$ estimation uses N_d = 1.28, π = 0.08[77]; inserted refs are for experimental BPs.

[a] Aqueous rates measured for hydroxyl plus TFA (M^{-1} s^{-1})[78]

[b] Gas-phase reaction of excess ·OH + perfluoropropene at 295 K[79]

[c] Gas-phase reaction of H· + CF_3CHFCF_3 – H· abstraction (cm^3 $molecule^{-1}s^{-1}$)[80]

[d] Calculated by bond-contribution method[81]

Table 3.3. Kinetic parameters for the unimolecular decomposition of fluorochemicals

Reaction	log A s^{-1}	E_A kJ mol^{-1}	k (T = 2500 K) s^{-1}	$\tau_{1/2}$ (ns)	ref.
$C_3F_7H \rightarrow CF_3\cdot + CF_2HCF_2\cdot$	16.9	372.6	1.29E+09	0.5	[68]
$C_3F_7H \rightarrow CHF_2\cdot + CF_3CF_2\cdot$	16.6	372.6	6.47E+08	1.1	[68]
$C_3F_7H \rightarrow HF + C_3F_6$	13.9	280.5	1.29E+06	540	[68]
$C_4F_8 \rightarrow CF_3\cdot + C_3F_5$	16.1	292.9	9.48E+09	0.07	[69]
$C_4F_8 \rightarrow C_3F_6 + CF_2$	13.0	380.7	1.10E+05	6,300	[69]
$C_4F_8 \rightarrow C_2F_4 + C_2F_4$	13.0	418.4	1.79E+04	39,000	[69]
$C_6F_{14} \rightarrow C_2F_5\cdot + C_4F_9$	17.2	330	2.00E+10	0.03	[53]
$C_6F_{14} \rightarrow 2\ C_3F_7\cdot$	16.9	330	1.00E+10	0.07	[53]
$C_6F_{14} \rightarrow CF_3\cdot + C_5F_{11}\cdot$	17.2	364	3.90E+09	0.18	[53]
$C_5F_{11}\cdot \rightarrow C_3F_7\cdot + C_2F_4$	13.6	168	1.22E+10	0.06	[53]
$C_4F_9\cdot \rightarrow C_2F_5\cdot + C_2F_4$	13.4	168	7.73E+09	0.09	[53]
$C_3F_7\cdot \rightarrow CF_3\cdot + C_2F_4$	13.3	186.4	2.53E+09	0.27	[53]
$C_3F_7\cdot \rightarrow C_2F_5\cdot + CF_2$:	15.5	238.4	3.28E+10	0.02	[53]
$C_2F_5\cdot \rightarrow CF_3\cdot + CF_2$:	15.6	235.4	4.78E+10	0.01	[53]
$C_2F_4 \rightarrow 2\ CF_2$:	16.7	294	3.58E+10	0.02	[53]

* $k = A\ T^b \exp(-E_A / RT)$ where E_A is in kJ mol^{-1}, R = 0.00831 kJ K^{-1} mol^{-1}, and A and thus k is in s^{-1}; in all cases b = 0.

Table 3.4. Kinetic parameters for bimolecular reactions of C_1-fluororadicals

Reaction	A molecule cm^{-3} s^{-1}	b	E_A kJ mol^{-1}	k (T = 4000 K) molecule cm^{-3} s^{-1}
$CHF_2\cdot + H \rightarrow CH_2F_2$	2.75E+06	-0.32	32.2	1.22E-19
$CHF_2\cdot + H \rightarrow CHF: + HF$	1.50E+14	-0.11	0.5	9.85E-11
$CHF_2\cdot + H \rightarrow CF_2: + H_2$	5.50E+03	2.41	0	4.38E-12
$CHF_2\cdot + OH \rightarrow CHF:O + HF$	2.40E+13	0	0	3.99E-11
$CHF_2\cdot + O \rightarrow CF_2:O + H$	3.70E+13	0	0	6.14E-11
$CF_3\cdot + H \rightarrow CF_2: + HF$	5.50E+13	0	0	9.13E-11
$CF_3\cdot + OH \rightarrow CF_2:O$	2.00E+13	0	0	3.32E-11
$CF_3\cdot + O \rightarrow CF_2:O + F$	1.90E+13	0	0	3.16E-11
$CF_2: + H_2O \rightarrow CHF:O + HF$	5.00E+12	0	104.6	3.57E-13
$CF_2: + OH \rightarrow CF:O + HF$	4.00E+12	0	14.6	4.28E-12
$CF_2: + OH \rightarrow CF_2:O + H$	2.00E+13	0	14.6	2.14E-11
$CF_2: + H \rightarrow CF + HF$	2.00E+14	0	14.6	2.14E-10
$CF_2: + O \rightarrow CF:O + F$	7.00E+13	0	4.2	1.02E-10
$CF + H_2O \rightarrow CHF:O + H$	2.00E+13	0	71.1	3.91E-12
$CF + OH \rightarrow CO + HF$	4.00E+13	0	4.2	5.85E-11
$CF + H \rightarrow CH + F$	4.00E+13	0	2.8	6.11E-11
$CF + O \rightarrow CO + F$	4.00E+13	0	4.2	5.85E-11
$CHF: + H_2O \rightarrow CH_2O + HF$	5.00E+12	0	27.2	3.66E-12
$CHF: + OH \rightarrow CHO + HF$	4.00E+12	0	0	6.64E-12

$CHF: + OH \rightarrow CFH:O + H$	2.00E+13	0	0	3.32E-11
$CHF: + H \rightarrow CH + HF$	3.00E+14	0	0	4.98E-10
$CHF: + O \rightarrow CO + HF$	9.00E+12	0	12.9	1.01E-11
$CHF:O + M \rightarrow CO + HF$	2.50E+25	-3	179.8	2.90E-12
$CHF:O + H \rightarrow CF:O + H_2$	1.10E+08	1.77	12.5	2.98E-10
$CHF:O + OH \rightarrow CF:O + H_2O$	1.70E+09	1.18	0	5.03E-11
$CHF:O + O \rightarrow CF:O + OH$	9.00E+12	0	12.9	1.01E-11
$CF_2:O + H_2O \rightarrow CO_2 + 2\ HF$	7.40E-03	3.84	105	3.54E-14
$CF_2:O + H \rightarrow CF:O + HF$	1.20E+10	0.83	93.3	1.18E-12
$CF_2:O + OH \rightarrow CO_2 + HF + F$	2.70E+03	2.38	87.8	1.20E-13
$CF:O + H \rightarrow CO + HF$	1.20E+14	0	0	1.99E-10
$CF:O + OH \rightarrow CO_2 + HF$	3.00E+13	0	0	4.98E-11
$CF:O + O \rightarrow CO_2 + F$	3.00E+13	0	0	4.98E-11
$F + H_2O \rightarrow HF + OH$	1.30E+09	1.5	0	5.46E-10
$F + H_2 \rightarrow HF + H$	2.60E+12	0.5	0	2.73E-10
$F + OH \rightarrow HF + O$	2.00E+13	0	0	3.32E-11

Table 3.5. Estimated CO/CO_2 product ratios for PFOX sonolysis

	Case I			Case II			Case III		
Water Vapor %	10.0	1.0	0.1	10.0	1.0	0.1	10.0	1.0	0.1
Radical %	1.0	1.0	1.0	0.1	0.1	0.1	Range	Range	Range
CFO									
CO/CO_2	2.00	2.00	2.00	2.00	2.00	2.00	0.40	0.40	0.40
CF_2O									
CO/CO_2	0.90	1.43	1.52	0.19	0.90	1.43	0.06	0.14	0.16
CHF									
CO/CO_2	94.73	89.33	88.79	750.99	479.89	452.78	23.53	17.13	16.49
CHFO									
CO/CO_2	4.43	4.43	4.43	26.32	26.32	26.32	5.45	5.45	5.45
$PFOS^-$									
CO/CO_2	5.21	6.66	6.87	4.63	5.99	6.79	1.05	1.21	1.25
Calc/Expt	1.02	1.31	1.35	0.91	1.17	1.33	0.21	0.24	0.25
$PFOA^-$									
CO/CO_2	2.48	2.85	2.90	2.20	2.69	2.94	0.78	0.86	0.89
Calc/Expt	1.24	1.43	1.45	1.10	1.35	1.47	0.39	0.43	0.44

References

(1) 3M Company. Docket AR226-0547; Office of Pollution Prevention and Toxics; U.S. Environmental Protection Agency: Washington, D.C., 1999; p. 12.

(2) Sinclair, E.; Kannan, K. *Environ. Sci. Technol.* **2006**, *40*, 1408.

(3) Schultz, M. M.; Higgins, C. P.; Huset, C. A.; Luthy, R. G.; Barofsky, D. F.; Field, J. A. *Environ. Sci. Technol.* **2006**, *40*, 7350.

(4) Boulanger, B.; Vargo, J. D.; Schnoor, J. L.; Hornbuckle, K. C. *Environ. Sci. Technol.* **2005**, *39*, 5524.

(5) Martin, J. W.; Whittle, D. M.; Muir, D. C. G.; Mabury, S. A. *Environ. Sci. Technol.* **2004**, *38*, 5379.

(6) Martin, J. W.; Smithwick, M. M.; Braune, B. M.; Hoekstra, P. F.; Muir, D. C. G.; Mabury, S. A. *Environ. Sci. Technol.* **2004**, *38*, 373.

(7) Schultz, M. M.; Barofsky, D. F.; Field, J. A. *Environ. Eng. Sci.* **2003**, *20*, 487.

(8) Key, B. D.; Howell, R. D.; Criddle, C. S. *Environ. Sci. Technol.* **1998**, *32*, 2283.

(9) Hollingsworth, J.; Sierra-Alvarez, R.; Zhou, M.; Ogden, K. L.; Field, J. A. *Chemosphere* **2005**, *59*, 1219.

(10) 3M Company; Docket AR226-0489; Office of Pollution Prevention & Toxics; U.S. Environmental Protection Agency: Washington, D.C., 1978; p. 19.

(11) 3M Company; Docket AR226-0058; Office of Pollution Prevention & Toxics; U.S. Environmental Protection Agency: Washington, D.C., 1994; p. 4.

(12) Oppenlander, T. *Photochemical Purification of Water and Air*; Wiley-VCH: Weinheim, 2003.

(13) Schroder, H. F.; Meesters, R. J. W. *J. Chromatogr. A* **2005**, *1082*, 110.

(14) Moriwaki, H.; Takagi, Y.; Tanaka, M.; Tsuruho, K.; Okitsu, K.; Maeda, Y. *Environ. Sci. Technol.* **2005**, *39*, 3388.

(15) Hori, H.; Hayakawa, E.; Einaga, H.; Kutsuna, S.; Koike, K.; Ibusuki, T.; Kiatagawa, H.; Arakawa, R. *Environ. Sci. Technol.* **2004**, *38*, 6118.

(16) Chen, J.; Zhang, P. *Water Sci. Technol.* **2006**, *54*.

(17) 3M Company; Docket AR226-0056; Office of Pollution Prevention & Toxics; U.S. Environmental Protection Agency: Washington, D.C., 1978; p. 17.

(18) 3M Company; Docket AR226-0490; Office of Pollution Prevention & Toxics; U.S. Environmental Protection Agency: Washington, D.C., 1979; p. 15.

(19) Yamamoto, T.; Noma, Y.; Sakai, S. I.; Shibata, Y. *Environ. Sci. Technol.* **2007**, *41*, 5660.

(20) Chen, J.; Zhang, P. Y.; Liu, J. *J. Environ. Sci* **2007**, *19*, 387.

(21) Hori, H.; Yamamoto, A.; Hayakawa, E.; Taniyasu, S.; Yamashita, N.; Kutsuna, S.; Kiatagawa, H.; Arakawa, R. *Environ. Sci. Technol.* **2005**, *39*, 2383.

(22) Hori, H.; Yamamoto, A.; Kutsuna, S. *Environ. Sci. Technol.* **2005**, *39*, 7692.

(23) Kutsuna, S.; Hori, H. *Int. J. Chem. Kin.* **2007**, 276.

(24) Chen, J.; Zhang, P. Y.; Zhang, L. *Chem. Lett.* **2006**, *35*, 230.

(25) Hori, H.; Hayakawa, E.; Koike, K.; Einaga, H.; Ibusuki, T. *J. Mol. Catal. A–Chem.* **2004**, *211*, 35.

(26) Dillert, R.; Bahnemann, D.; Hidaka, H. *Chemosphere* **2007**, *67*.

(27) Yuan, Q.; Ravikrishna, R.; Valsaraj, K. T. *Sep. Purif. Technol.* **2001**, *24*.

(28) Hidaka, H.; Jou, H.; Nohara, K.; Zhao, J. *Chemosphere* **1992**, *25*, 1589.

(29) Hori, H.; Nagaoka, Y.; Yamamoto, A.; Sano, T.; Yamashita, N.; Taniyasu, S.; Kutsuna, S.; Osaka, I.; Arakawa, R. *Environ. Sci. Technol.* **2006**, *40*, 1049.

(30) Kolaczkowski, S. T.; Plucinski, P.; Beltran, F. J.; Rivas, F. J.; McLurgh, D. B. *Chem. Eng. J.* **1999**, *73*, 143.

(31) Vinodgopal, K.; Ashokkumar, M.; Grieser, F. *J. Phys. Chem. B* **2001**, *105*, 3338.

(32) Destaillats, H.; Hung, H. M.; Hoffmann, M. R. *Environ. Sci. Technol.* **2000**, *34*, 311.

(33) Hua, I.; Hoffmann, M. R. *Environ. Sci. Technol.* **1996**, *30*, 864.

(34) Kotronarou, A.; Mills, G.; Hoffmann, M. R. *J. Phys. Chem.* **1991**, *95*, 3630.

(35) Petrier, C.; David, B.; Laguian, S. *Chemosphere* **1996**, *32*, 1709.

(36) Brennen, C. E. *Cavitation and Bubble Dynamics*; Oxford University Press: New York, 1995.

(37) Misik, V.; Miyoshi, N.; Riesz, P. *J. Phys. Chem.* **1995**, *99*, 3605.

(38) Leighton, T. G. *The Acoustic Bubble*; Academic Press: London, 1994.

(39) Didenko, Y. T.; McNamara, W. B.; Suslick, K. S. *J. Phys. Chem. A* **1999**, *103*, 10783.

(40) Colussi, A. J.; Weavers, L. K.; Hoffmann, M. R. *J. Phys. Chem. A* **1998**, *102*, 6927.

(41) Storey, B. D.; Szeri, A. J. *Proc. R. Soc. London Ser. A–Math. Phys. Eng. Sci.* **2000**, *456*, 1685.

(42) Yasui, K.; Tuziuti, T.; Kozuka, T.; Towata, A.; Iida, Y. *J. Chem. Phys.* **2007**, *127*.

(43) Krishna, C. M.; Lion, Y.; Kondo, T.; Riesz, P. *J. Phys. Chem.* **1987**, *91*, 5847.

(44) Jennings, B. H.; Townsend, S. N. *J. Phys. Chem.* **1961**, *65*, 1574.

(45) Colussi, A. J.; Hung, H. M.; Hoffmann, M. R. *J. Phys. Chem. A* **1999**, *103*, 2696.

(46) Yang, L. M.; Rathman, J. F.; Weavers, L. K. *J. Phys. Chem. B* **2005**, *109*, 16203.

(47) Sostaric, J. Z.; Riesz, P. *J. Am. Chem. Soc.* **2001**, *123*, 11010.

(48) Henglein, A.; Kormann, C. *Int. J. Radiat. Biol.* **1985**, *48*, 251.

(49) Manousaki, E.; Psillakis, E.; Kalogerakis, N.; Mantzavinos, D. *Water Res.* **2004**, *38*, 3751.

(50) Glockner, V.; Lunkwitz, K.; Prescher, D. *Tenside Surf. Det.* **1989**, *26*.

(51) Krusic, P. J.; Marchione, A. A.; Roe, D. C. *J. Fluor. Chem.* **2005**, *126*, 1510.

(52) Lazerte, J. D.; Hals, L. J.; Reid, T. S.; Smith, G. H. *J. Am. Chem. Soc.* **1953**, *75*, 4525.

(53) Ainagos, A. F. *Kinet. Catal.* **1991**, *32*, 720.

(54) Harada, H. *Ultrason. Sonochem.* **1998**, *5*, 73.

(55) Henglein, A. *Z. Naturforsch. (B)* **1985**, *40*, 100.

(56) Lopez-Fontan, J. L.; Gonzalez-Perez, A.; Costa, J.; Ruso, J. M.; Prieto, G.; Schulz, P. C.; Sarmiento, M. *J. Colloid Interface Sci.* **2006**, *294*, 458.

(57) Lopez-Fontan, J. L.; Sarmiento, F.; Schulz, P. C. *Colloid Polym. Sci.* **2005**, *283*, 862.

(58) Simister, E. A.; Lee, E. M.; Lu, J. R.; Thomas, R. K.; Ottewill, R. H.; Rennie, A. R.; Penfold, J. *J. Chem. Soc.–Faraday Trans.* **1992**, *88*, 3033.

(59) Shinoda, K.; Hato, M.; Hayashi, T. *J. Phys. Chem.* **1972**, *76*, 909.

(60) Lesko, T.; Colussi, A. J.; Hoffmann, M. R. *Environ. Sci. Technol.* **2006**, *40*, 6818.

(61) Lines, D.; Sutcliffe, H. *J. Fluor. Chem.* **1984**, *25*, 505.

(62) Krusic, P. J.; Roe, D. C. *Anal. Chem.* **2004**, *76*, 3800.

(63) Hung, H. M.; Hoffmann, M. R. *Environ. Sci. Technol.* **1998**, *32*, 3011.

(64) Hung, H. M.; Hoffmann, M. R. *J. Phys. Chem. A* **1999**, *103*, 2734.

(65) Goss, K. U.; Bronner, G. *J. Phys. Chem. A* **2006**, *110*, 9518.

(66) Goss, K. U.; Bronner, G.; Harner, T.; Monika, H.; Schmidt, T. C. *Environ. Sci. Technol.* **2006**, *40*, 3572.

(67) Goss, K.-U. *Environ. Sci. Technol.* **2008**, *42*, 456.

(68) Kato, S.; Makide, Y.; Tominaga, T.; Takeuchi, K. *J. Phys. Chem.* **1987**, *91*, 4278.

(69) Longfellow, C. A.; Berrie, C. L.; Suits, A. G.; Lee, Y. T. *J. Chem. Phys.* **1997**, *107*, 7202.

(70) Ciawi, E.; Rae, J.; Ashokkumar, M.; Grieser, F. *J. Phys. Chem. B* **2006**, *110*, 13656.

(71) Didenko, Y. T.; McNamara, W. B.; Suslick, K. S. *J. Am. Chem. Soc.* **1999**, *121*, 5817.

(72) Burgess, D. R.; Zachariah, M. R.; Tsang, W.; Westmoreland, P. R. *Prog. Energy Combust. Sci.* **1995**, *21*, 453.

(73) Destaillats, H.; Lesko, T. M.; Knowlton, M.; Wallace, H.; Hoffmann, M. R. *Ind. Eng. Chem. Res.* **2001**, *40*, 3855.

(74) Galyautdinov, I. V.; Nazmeeva, S. R.; Savchenko, R. G.; Ves'kina, N. A.; Nedopekin, D. V.; Fatykhov, A. A.; Khalilov, L. M.; Odinokov, V. N. *Russ. J. Organ. Chem.* **2004**, *40*, 675.

(75) Huang, B. N.; Haas, A.; Lieb, M. *J. Fluor. Chem.* **1987**, *36*, 49.

(76) Mackay, D.; Bobra, A.; Chan, D. W.; Shiu, W. Y. *Environ. Sci. Technol.* **1982**, *16*, 645.

(77) Schwarzenbach, R. P.; Gschwend, P. M.; Imboden, D. M. *Environmental Organic Chemistry*, *Second ed.*; Wiley: New York, 2003.

(78) Maruthamuthu, P.; Padmaja, S.; Huie, R. E. *Int. J. Chem. Kin.* **1995**, *27*.

(79) Mashino, M.; Ninomiya, Y.; Kawasaki, M.; Wallington, T. J.; Hurley, M. D. *J. Phys. Chem. A* **2000**, *104*, 7255.

(80) Yamamoto, O.; Takahashi, K.; Inomata, T. *J. Phys. Chem. A* **2004**, *108*, 1417.

(81) Hine, J.; Mookerjee, P. K. *J. Org. Chem.* **1975**, *40*, 292.